

We are IntechOpen, the world's leading publisher of Open Access books Built by scientists, for scientists

6,900

Open access books available

186,000

International authors and editors

200M

Downloads

Our authors are among the

154

Countries delivered to

TOP 1%

most cited scientists

12.2%

Contributors from top 500 universities



WEB OF SCIENCE™

Selection of our books indexed in the Book Citation Index
in Web of Science™ Core Collection (BKCI)

Interested in publishing with us?
Contact book.department@intechopen.com

Numbers displayed above are based on latest data collected.
For more information visit www.intechopen.com



Nanocomposite Thin Films Resulting from Au Nanoclusters Dispersed in a Titanium Oxide Dielectric Matrix: the Surface Plasmon Resonance Effect

M. Torrell¹, L. Cunha¹, M.I. Vasilevskiy¹, E. Alves²,
N.P. Barradas², A. Cavaleiro³ and F. Vaz¹

¹Universidade do Minho, Centro de Física, Braga,

²Instituto Tecnológico e Nuclear and CFN da Universidade de Lisboa, Sacavém,

³SEC-CEMUC – Universidade de Coimbra, Dept. Eng. Mecânica, Pólo II, Coimbra,
Portugal

1. Introduction

The increasing interest of the scientific community in the nanocomposite thin films containing noble metal nanoparticles (MNP) embedded in dielectric matrices is related to a relatively wide range of possible applications. Although it may sound strange, the awareness of the properties and applications of this kind of nanocomposites already existed many centuries ago. To begin with, MNP provided different colours in Roman glasses, as the well-known Lycurgus Cup from the third century, which nowadays can be visited in the British Museum of London. Another remarkable example of this ancient use of this kind of nanocomposite system is the on the fabrication of medieval cathedrals' windows that were decorated with noble metal powders (commonly from Au). For certain powder conditions, the addition would give rise to astonishing effects on the cathedral windows, namely in certain tones of blue and red that could be obtained. This was done during centuries. More recently, the use of these films on high value consumer goods is gaining increasing interest, namely for decorative applications, jewellery and some domestic technological devices and furniture.

The rapid development of different preparation approaches and the increasing knowledge that is becoming available from the study of the scientific content that is involved in these nanocomposites, together with a detailed characterisation of their main properties, is bringing an increasing amount of new and modern applications, beyond those of purely decorative purposes. Among the new possibilities, it worth mention those related with the fabrication of colour filters (Takele et al, 2006) bio- and optical sensors (Hutter & Fendler, 2004; Walters & Parkin, 2008; Torrell et al., 2010a), absorption elements of solar cells (Walters & Parkin 2008), enhancement of electrical/thermal conductivity of coatings, photocatalytic antibacterials (Wang et al., 2006a), pollutant-degradation materials (Pacholski et al., 2004; Wu & Tseng, 2006; Li et al., 2009), gas sensors (Atashbar et al., 1998; Walton et al., 1998), nonlinear optical devices (Walters & Parkin, 2008; Cho et al., 2000;

Hache et al., 1988) and the recent Surface Enhanced Raman Scattering effect (SERS) (Kim et al., 2010). Most of these applications rely on the tailoring of the so-called Surface Plasmon Resonance (SPR) absorption, which is highly dependent of the type of the noble metal that is selected (typically silver and gold), the possibility of the metallic atoms to form a network of clusters (at the nanometric scale), their correspondent morphology (size, shape and distribution behaviour), but also on the dielectric properties of the medium where the metallic nanoparticles (nanoclusters) are dispersed (Dalacu & Martinu, 1999; Cho et al., 2000; Dalacu & Martinu, 2000; Bohren & Huffman, 1998; Deng et al., 2008; Matsuoka et al., 1997; Liao et al. 1997; Mandal et al., 2002; Sella et al., 2009; Zhou et al., 2004).

The Surface Plasmon effect is defined as the collective oscillation of the free or conduction electrons, induced by an external electromagnetic field. As already mentioned above, this oscillation effect can be tuned by the changes on the nanocomposite morphology, especially in what concerns to the particular clustering size (at the nanometric scale), shape (spherical, elongated or even other more complicated forms) and distribution (either uniform or localized) (Dalacu & Martinu, 1999; Cho et al., 2000; Dalacu & Martinu, 2000). Other important factors are the distances of the metallic particles in the dielectric medium, which can be changed by changing their matrix populations, and the crystallographic structure of the dielectric oxide matrix (Mandal et al., 2002; Cho et al. 2004). A strong local field effect arises from the dielectric confinement and shows a maximum at the so-called SPR frequency, where the quantized collective motion of the confined free electrons is resonantly-coupled to the incident electromagnetic field, yielding characteristic absorption bands. This is exactly the basis for most of the upper referred application possibilities and examples. However, only metals with free electrons, and in particular those from the eleventh group elements of the periodic table (e.g. Au, Ag and Cu), possess Plasmon Resonances in the visible spectrum (Liz-Marzan, 2004), and thus restricting the available possibilities. This group of metals offer a quasi-free-electron behaviour on the UV-visible range, resulting, for example, in intense and attractive colourations.

The methods to fabricate these nanocomposite thin films, where metallic nanoparticles are dispersed in non-aqueous dielectric media (latex, polystyrene, TiO₂, SiO₂, among others), using for example Physical Vapour Deposition methods (PVD) or Chemical Vapour Deposition methods (CVD), is actually becoming one of the most important fields in specific areas of materials science, integrating a new aim for the use of nanoscience and nanotechnology (Walters & Parkin, 2008; Wang et al., 2006b; Armelao et al., 2006). PVD-based methods, such as reactive magnetron sputtering, have become established in the actual market as an important competitor to classic electrochemical processes (Navinsek et al., 1999; Fenker et al., 2004). The great advantage is that they allow overcoming the highly restrictive normative, namely the environmental ones, that are being applied on the decorative and protector electrochemical films industry.

Taking all the above considerations into account, this chapter intends to give a small contribute to the basic knowledge on the preparation, characterization and performance of nanocomposites coatings, consisting of gold nanoclusters dispersed in a titanium oxide dielectric matrix. Due to the high degree of flexibility on the basic preparation parameters, associated to an easy up scaling of the laboratory-based work to industrial environment, the reactive magnetron sputtering (DC) method was selected for the preparation of the nanocomposites, in the form of thin solid films. The tailoring of the SPR effect (the change on the size, shape and distribution of the noble metal - gold, clusters) was carried out by the application of an after deposition thin film annealing protocol.

2. Theoretical background

Surface Plasmon Resonance, SPR, in Metallic NanoParticles, MNP, is the result of the collective oscillations of the free electrons, induced by an external electromagnetic radiation. Its spectral characteristics depend on both MNP and host matrix properties. Let us recall the essential SPR features in a single metallic particle embedded in a dielectric matrix by considering a perfectly spherical particle and the dipole approximation of the Mie theory (Mie, 1908). This approximation is valid particles with a radius significantly smaller than the wavelength of the incident electromagnetic radiation. The Surface Plasmon Resonance condition is then given by:

$$\varepsilon_s + 2\varepsilon_h = 0 \quad (1)$$

where $\varepsilon_h = n_h^2$ is the dielectric constant of the host matrix and ε_s denotes the dielectric function of the metal. In the simple Drude model,

$$\varepsilon_s(\omega) = \varepsilon_\infty \left[1 - \frac{\omega_p^2}{\omega(\omega + i\Gamma_p)} \right] \quad (2)$$

where ε_∞ is a positive constant, and Γ_p is a Plasmon damping parameter (proportional to the electron scattering rate). This parameter depends on the nanoparticles size and has a direct and important effect on the width of a single SPR peak. For spherical Au nanoparticles, the following expression has been proposed (Mie, 1908):

$$\hbar\Gamma_p(R) = \hbar\Gamma_p(\text{bulk}) + g_s v_F / R = 0.0244 + 0.922g_s / R \quad [\text{eV}] \quad (3)$$

where v_F is the Fermi velocity, g_s is a geometrical factor of the order of unity, and R the nanoparticle radius (in nanometers). For the geometrical factor, a value of $g_s \approx 0.7$ has been suggested (Baida et al., 2009). The intensity of the resonance is inversely proportional to Γ_p and directly proportional to the particle volume (R^3).

$$\omega_p = \sqrt{4\pi n e^2 / (\varepsilon_\infty m^*)} \quad (4)$$

is the plasma frequency, where n corresponds to the free electron concentration and m^* denotes the effective mass. Assuming that $\Gamma_p \ll \omega_p$, Eqs. (1) and (2) enables to characterize the SPR frequency for a spherical nanoparticles, on the following form:

$$\omega_{SPR} = \frac{\omega_p}{\sqrt{1 + 2\varepsilon_h / \varepsilon_\infty}} \quad (5)$$

Equation (5) shows that the SPR spectral position is, in fact, independent of the nanoparticles size, but depending much on the dielectric constant of the host matrix. In order to achieve a SPR effect in the visible range, one is practically limited to the noble metals and still has to use host materials with sufficiently high dielectric constant. The width of the resonance is proportional to Γ_p , which increase for smaller particles due to an additional scattering mechanism, called surface scattering, becomes more important as R decreases. The intensity of the SPR peak is proportional to the particle volume.

The SPR characteristics are affected by the shape and orientation of the particles in the matrix if they are not spherical (Rodriguez-Fernandez et al. 2009). For example, axial-symmetric nanorods are supposed to produce two SPRs, with the characteristic frequencies given by:

$$\omega'_{SPR} = \frac{\omega_p}{\sqrt{1 + (\eta_{||}^{-1} - 1)\epsilon_h/\epsilon_\infty}} \text{ and } \omega''_{SPR} = \frac{\omega_p}{\sqrt{1 + (\eta_{\perp}^{-1} - 1)\epsilon_h/\epsilon_\infty}} \quad (6)$$

where $\eta_{||}$ and η_{\perp} are geometrical factors, commonly known as depolarization coefficients (Landau & Lifshitz, 1984), which correspond to some non-negative numbers obeying the relation:

$$\eta_{||} + 2\eta_{\perp} = 1 \quad (7)$$

The first resonance takes place for electromagnetic waves polarized along the nanorod axis, while the second corresponds to the perpendicular polarisation. If nanorods are embedded in a matrix in a random-orientation fashion, then one would expect to observe both SPRs. If matrix, in a random-orientation fashion, then one should expect we approximate nanorods by elongated (prolate) spheroids with eccentricity e , the depolarization coefficients are given by:

$$\eta_{||} = \frac{1 - e^2}{e^3} \left(\frac{1}{2} \log \frac{1 + e}{1 - e} - e \right) \leq \frac{1}{3} \quad (8)$$

$$\eta_{\perp} = \frac{1 - \eta_{||}}{2} \geq \frac{1}{3} \quad (9)$$

Using these relations one can see that $\omega'_{SPR} < \omega_{SPR} < \omega''_{SPR}$. The two resonances corresponding to Eq. (6) merge into a single one determined by Eq. (5), when $\eta_{||} = \eta_{\perp} = 1/3$ (spherical nanoparticles).

Inter-particle spacing (i.e., the particle concentration) can also have an effect on the SPR intensity, peak position and width. It is related to an electromagnetic dipole-dipole interaction between the nanoparticles. These effects become considerable when the volume fraction of the particles is above $\approx 10\%$. The theoretical predictions (Landau & Lifshitz, 1984; Ung et al., 2001) indicate that increased volume fraction of gold MNP raises the SPR intensity and leads to a red shift of the position of the resonance. A typical effect of the SPR effect is the red shift of the absorption band, which is related to a change in the phase composition of the matrix: the transition temperature of the anatase to rutile TiO_2 . The two phases have different values of the refractive index, reported as $n_{\text{anatase}} = 2.5$ and $n_{\text{rutile}} = 2.9$ at $\lambda = 550$ nm (Song et al., 2005).

A model of the optical properties of the Au: TiO_2 composite films was performed in order to quantify the previous arguments.

3. Optical spectra modelling

To describe the correlation between the morphological/structural changes of the films (promoted by an external input such as an annealing treatment) with the optical spectra of the nanocomposite films, theoretical models of the effective dielectric function using the

approaches known in the optics of composite and layered media the optical behaviour can be developed.

Considering that the wavelength of the electromagnetic radiation is much larger than both the particle size and the inter-particle distance, the composite medium can be described by an effective dielectric function (EDF). There are two well-known mean-field theories for the EDF calculation, proposed, respectively, by Maxwell-Garnett and Bruggemann (Genzel & Kreibig, 1980; Shalaev, 2000). The first one is valid in the low-concentration limit (volume fraction of the particles $f \ll 1$), while the second can be applied when both f and $(1-f)$ are not too small. Some further studies are published in the scientific bibliography (Genzel & Kreibig, 1980; Shalaev, 2000). For most of the nanocomposites usually studied, one has $f \approx 0.1$, and none of these classical approximations is suitable. The Maxwell-Garnett (MG) approximation (assuming independent polarisable particles) can be improved and, consequently, extended to higher f by taking into account the dipole-dipole interactions between the particles (Vasilevskiy & Anda, 1996; Vasilevskiy 2000). This formalism will be hereafter referred to as renormalized Maxwell-Garnett (RMG) approximation, since it considers a polarizability of the particles renormalized by their interactions (M. Torrell et al., 2010b). It is conceptually equivalent to the average T-matrix approximation known in the theory of disordered media (Shalaev, 2000). The RMG approach has been generalized to non-spherical particles in Ref. (Vasilevskiy & Anda, 1996).

An individual particle, polarized by the external electromagnetic field but not interacting with other particles, is described by a bare polarizability tensor with the principal components given by:

$$\alpha_i = \frac{\varepsilon_s/\varepsilon_h - 1}{(\varepsilon_s/\varepsilon_h - 1)\eta_i + 1} \left(\frac{V}{4\pi} \right) \quad i = 1, 2, 3. \quad (10)$$

Here V is the particle volume and η_i are the depolarization coefficients mentioned in the Introduction (two of them coincide if the particle possesses axial symmetry). For a spheroid with (small) eccentricity e , they are given by (Landau & Lifshitz, 1984):

$$\eta_{\perp} = \frac{1}{3} \mp \frac{1}{15} e^2, \quad i = 1, 2; \quad \eta_{\parallel} = \frac{1}{3} \pm \frac{2}{15} e^2, \quad i = 3, \quad (11)$$

where the two signs correspond to the prolate (elongated) and oblate shape, respectively.

Within the classical MG approximation, the effective dielectric function, ε^* , of the composite medium containing a small fraction of separate inclusions is obtained from the relation:

$$\frac{\varepsilon^* - \varepsilon_h}{\varepsilon^* + 2\varepsilon_h} = \frac{4\pi}{3} N \bar{\alpha}, \quad (12)$$

where $N = f/V$ is the particle's concentration and $\bar{\alpha} = \sum_i \alpha_i / 3$.

The dipole-dipole interaction between the particles renormalizes their average polarizability, which becomes:

$$\alpha^* = \frac{2\bar{\alpha}}{\gamma} \left\{ 1 - \frac{\sqrt{1-\gamma(1-\delta)}}{2} \left[\sqrt{1-\nu^2} + \frac{\arcsin(\nu)}{\nu} \right] \right\}, \quad (13)$$

$$\text{where } \nu^2 = \frac{3\gamma\delta}{1-\gamma(1-\delta)}, \quad \gamma = f\left(\frac{4\pi\bar{\alpha}}{3V}\right)^2 \quad \text{and} \quad \delta = \pm\left(\frac{e^2}{15}\right)\frac{\epsilon_s/\epsilon_h-1}{\epsilon_s/\epsilon_h+2}$$

Note that $\alpha^* \rightarrow \bar{\alpha}$ when $f \rightarrow 0$, Eq. (13) is valid for uniform size particles and the more sophisticated formulae, taking into account the nanoparticles size dispersion, can be found in Ref. (Vasilevskiy & Anda, 1996). The effective dielectric function within the RMG approach is calculated by Eq. (12) with α^* replacing $\bar{\alpha}$. Once the dielectric function $\epsilon^*(\omega)$ is described it is possible to calculate the optical properties of the thin film nanocomposites. For thin films the eventual multiple reflections at the interface(s) have to be taken into account, causing the interference effect also detected in these materials for low concentrations of nanoparticles or very small sizes. When the dielectric functions of the film and the substrate are known, the most convenient method is to use the transfer matrix formalism to calculate the transmission and reflection spectra.

Calculated absorption spectra are presented in figures 1 through 3. As one can see from figure 1, the dipole-dipole interaction (taken into account within the RMG approach) becomes increasingly important as the volume fraction of Au nanoparticles increases. All the other results shown were obtained using the RMG approximation.

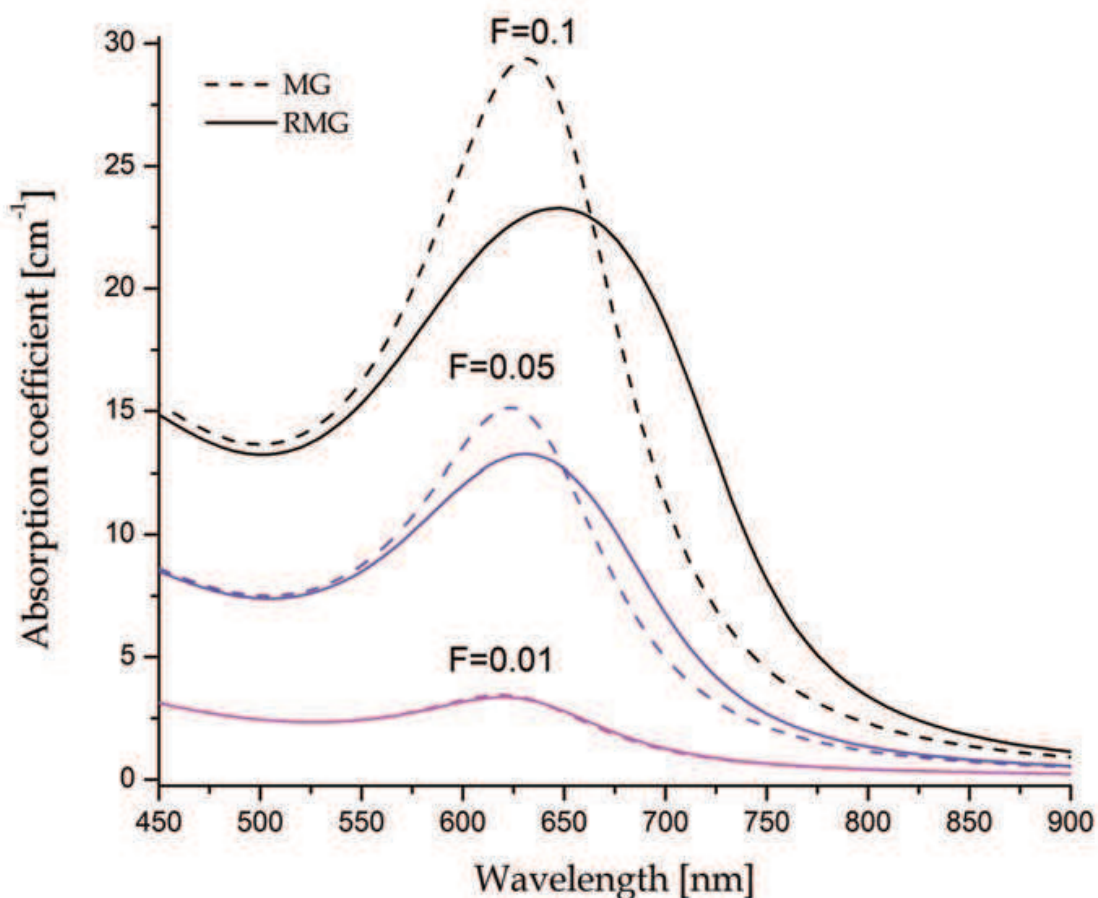


Fig. 1. Simulation of the absorption spectra of Au:TiO₂ nanocomposites with different volume fraction of Au considering spherical clusters of 10 nm, calculated using the standard MG and RMG approximations.

Figure 2 shows that a decrease of the mean nanoparticles radius, $\langle R \rangle$, results in a broader absorption spectrum while the peak position remains practically unshifted. Contrary to what one might expect, size dispersion does not produce an additional inhomogeneous broadening of the absorption band (as it is typical of semiconductor nanoparticles). On the contrary, the absorption peak becomes slightly narrower and higher. For the same $\langle R \rangle$, a broader size distribution increases the number of large nanoparticles, which absorb more strongly (notice that $\bar{\alpha}$ is proportional to the volume) and are characterized by a smaller homogeneous broadening.

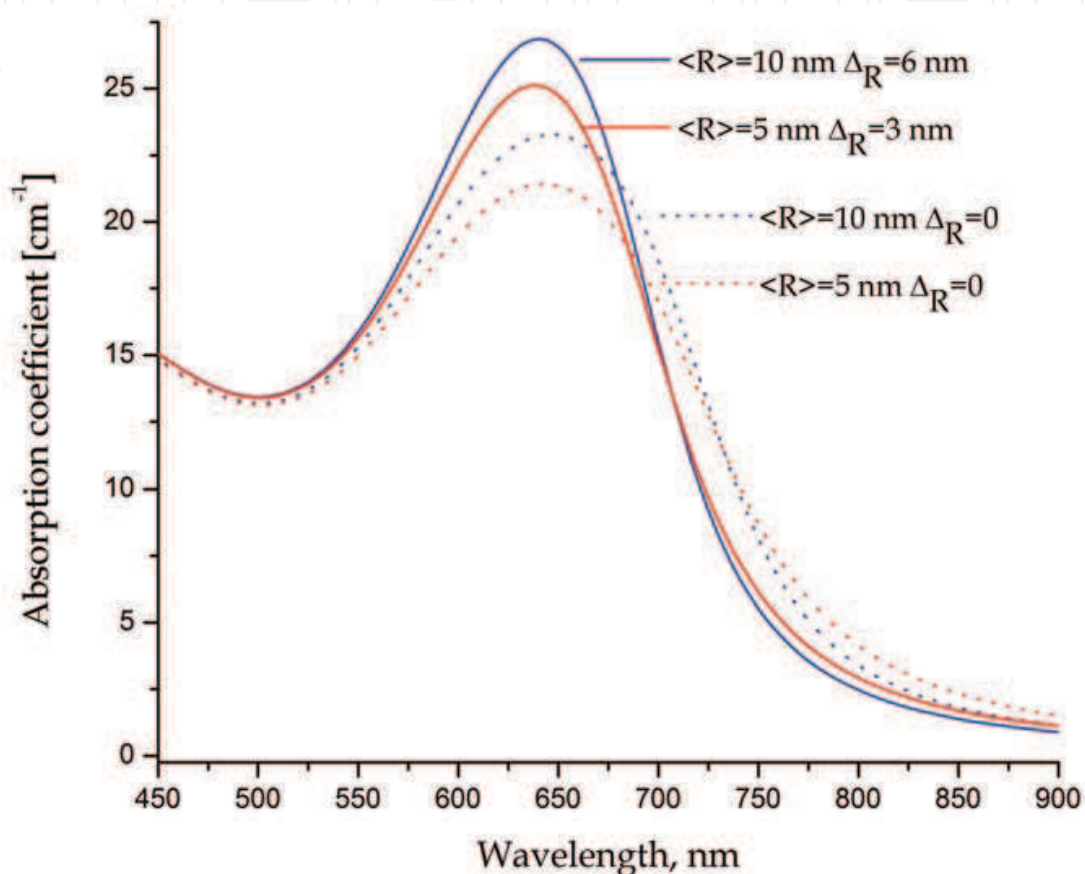


Fig. 2. Simulation of absorption spectra of nanocomposites containing Au spherical nanoparticles of different mean radius and size dispersion.

Figure 3 demonstrates the effect of nanoparticles shape on the SPR. It is clearly seen that there are two separate resonances already for moderately elongated nanoparticles ($e = 0.75$ corresponds to an aspect ratio of just 1.25). For nanorods $\eta_{\parallel} \rightarrow 0$ and the low-frequency SPR should be strongly red-shifted with respect to ω_{SPR} characteristic of spherical nanoparticles.

4. Nanocomposite films production and characterization techniques

It has been demonstrated that one of the easiest methods to produce nanocomposites thin films of noble metal nanoparticles embedded in dielectric matrix is the magnetron sputtering technology. In this chapter, a one-step deposition has been used to produce the host dielectric matrix (TiO_2) and the gold nanoparticles.

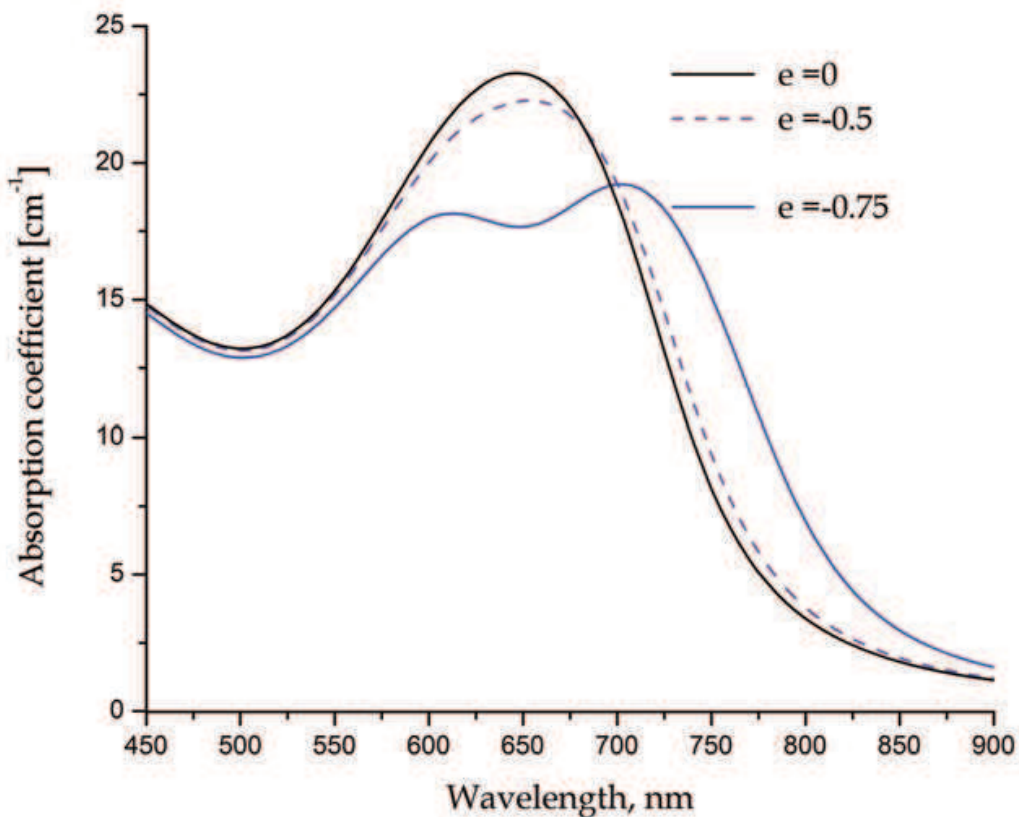


Fig. 3. Simulation of the absorption spectra of nanocomposites containing Au nanoparticles of spherical shape with different eccentricity.

To deposit a batch of Au:TiO₂ thin films onto silicon (100) and quartz substrates, a laboratory-sized magnetron PVD deposition apparatus was used. The rectangular magnetrons were disposed vertically in a closed field configuration in the deposition chamber. Only one electrode was powered, composed of a titanium target (99.6 % purity), with different amounts of Au pellets (with a 40 mm² surface area and approximately 2 mm thickness), symmetrically incrustated in its preferential erosion zone. A constant dc current density of 100 A m⁻² was applied. A mixture of argon and oxygen was injected with constant fluxes of 60 sccm and 10 sccm, corresponding to partial pressures of 0.3 Pa and 0.08 Pa, respectively. The final working pressure (\approx 0.38 Pa) and deposition temperature (about 150 °C) were kept approximately constant during the entire coating deposition process. The temperature of the coated substrates was monitored with a thermocouple placed close to the surface of the substrate holder.

Samples were placed in a rotating substrate holder in grounded condition. All samples were heat treated through annealing experiments in vacuum, after film deposition. Annealing treatments were carried out in a secondary vacuum furnace, after its evacuation to about 10⁻⁴ Pa. The selected temperature range varied from 200 to 800 °C, and the isothermal period was fixed to 60 min, after a heating ramp of 5 °C/min. The samples cooled down freely in vacuum before their removal to room conditions. The chemical uniformity and the atomic composition of the as-deposited samples were measured by Rutherford Backscattering Spectroscopy (RBS) using either a 1.4 or 1.75 MeV proton beam and a 2 MeV ⁴He. The scattering angles were 140° (standard detector, IBM geometry) and 180° (annular detector), and the incidence angle was varied between 0 and 30°. Composition profiles for the as-

deposited samples were generated using software code NDF (Barradas et al., 1997). For the ^{16}O data, the cross-sections given by Gurbich (Gurbich, 1997) were used. The analyzed area was about $0.5 \times 0.5 \text{ mm}^2$. In addition, for some samples, Particle Induced X-ray Emission (PIXE) measurements were performed to check for impurities.

All coatings were characterized by X-ray diffraction (XRD), using a Philips PW 1710 diffractometer (Cu-K α radiation), operating in a Bragg-Brentano configuration. XRD patterns were deconvoluted assuming to be Voigt functions to yield the peak position, integrated intensity and integrated width (IntW). The average nanoparticles size was determined by three different methods (Integral Breath, Fourier analysis, and Scherrer formula), using the Au-fcc (111) peak parameters obtained from the XRD patterns. The thickness and morphology of the films were studied by NanoSEM FEI Nova 200 scanning microscopy and transmission electron microscopy (TEM) using a Hitachi 800H apparatus. TEM microscopy has been used also to characterize the shape, size and distribution of Au nanoparticles with respect to the annealing temperature. Optical properties (Transmittance-absorbance) were characterized using a UV-Vis-NIR Spectrophotometer (Shimadzu UV 3101 PC) in the spectral range from 200 nm to 900 nm. SEM images of the coatings have been obtained by a NanoSEM FEI Nova 200 scanning microscopy.

5. Experimental results and discussion

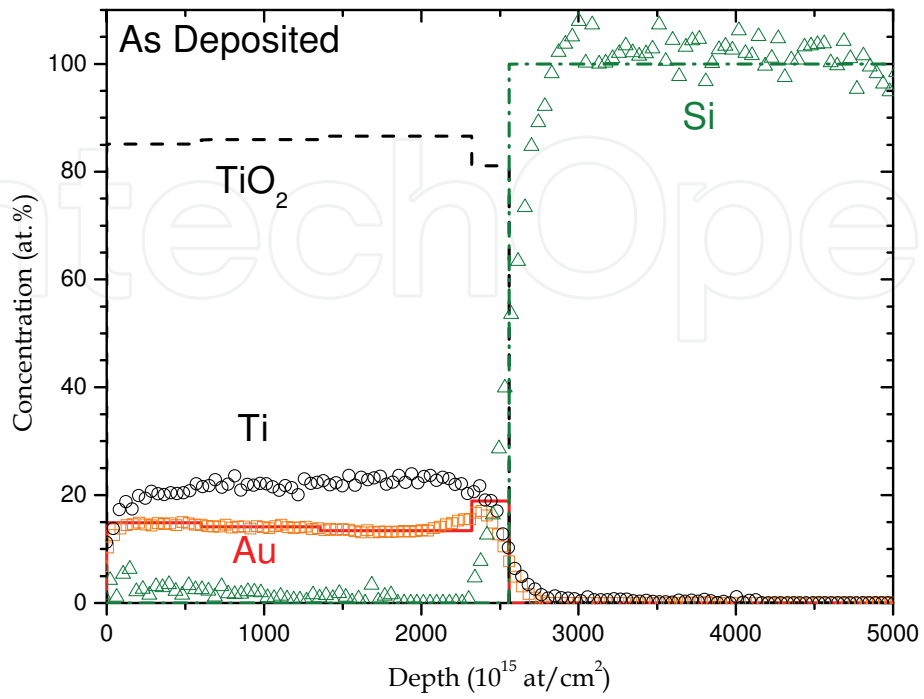
5.1 Composition and structure

The Au concentration in the samples, studied by RBS, was found to be close to 12 at. %. The elemental concentration analysis also revealed that the ratio O/Ti was always very close to 2, which suggests the presence of a stoichiometric-like TiO_2 matrix, with no apparent variation during the annealing experiments (as far as it concerns the resolution of the measurement techniques). The optimum Au nanoparticles concentration that was placed in the films has been previously studied and published. The Au volume fraction, f_{Au} , was determined as being close to 0.18 (considering $\rho(\text{Au}) = 19.3 \text{ g/cm}^3$ and $\rho(\text{TiO}_2) = 4 \text{ g/cm}^3$). It was already known, that for this type of nanocomposites, the range between 10 and 20 at. % Au conducted to the highest and most evident SPR activity on the optical properties (Armelaio et al., 2006).

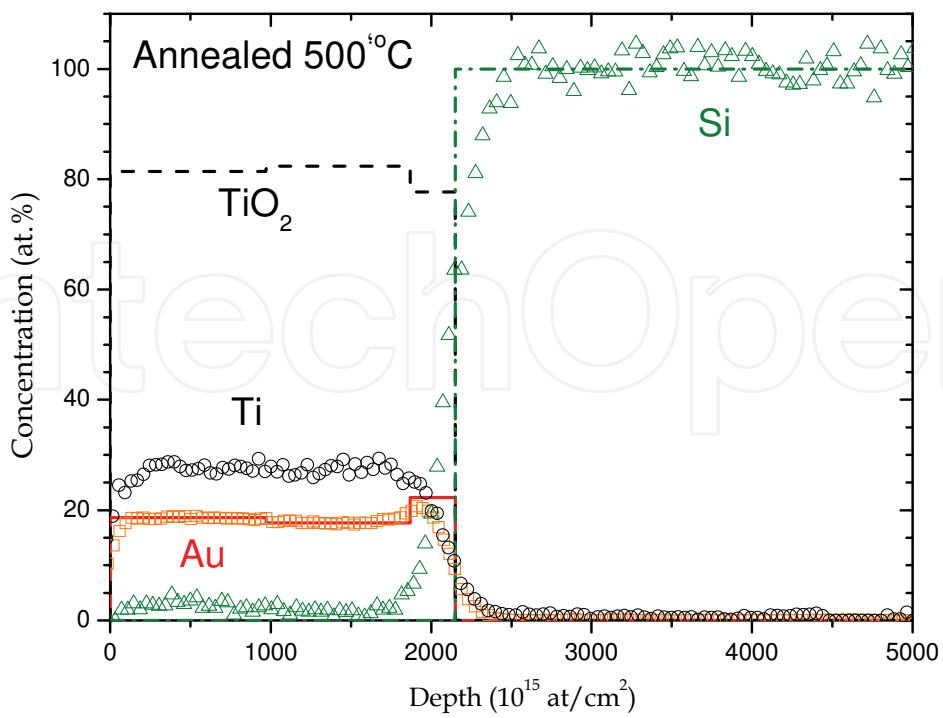
Beyond the annealing treatment, onset of a composition gradient could be expected due to enhanced Au diffusion into the substrate (Alves et al., 2011). However, it is not seen until the $800 \text{ }^\circ\text{C}$ annealing temperature as revealed by the RBS analysis (Figure 4). For temperatures up to $700 \text{ }^\circ\text{C}$, the composition profile analysis indicates that the samples are practically homogeneous across the film thickness. These results can have an influence on the optical properties of the films.

Measurements of the coatings thickness were carried out by scanning electron microscopy observation (cross-section view, figure 5). The cross section confirms that the films have approximately 300 nm. The cross-section micrograph shown in Fig. 5 reveals that the film grows in a compact and dense featureless structure, without any special growing characteristics (featureless growth).

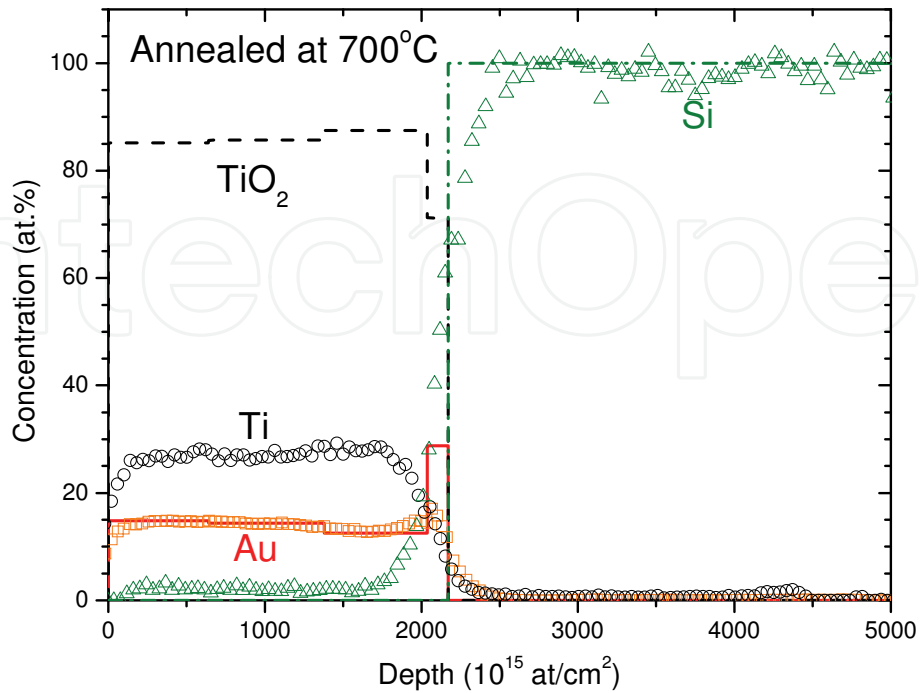
In spite of the small round features observed in SEM micrographs, the use of backscattering electron images undoubtedly showed that no signs of Au agglomerations were detected (in the as-deposited films), at least within the 2 nm maximum lateral resolution of the used SEM instrument. From SEM micrographs, one cannot take any conclusive results from the annealed samples, which show very similar results, without any clear evidences in the



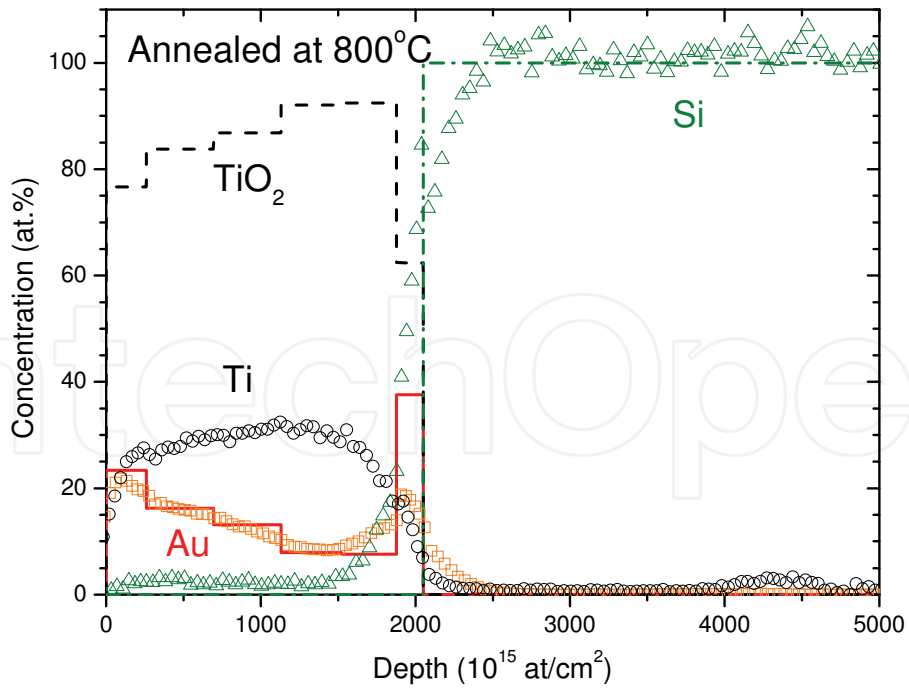
a)



b)



d)



e)

Fig. 4. Concentration profile of the nanocomposite annealed at: a) As Deposited b) 500°C d)700 °C and e) 800 °C.

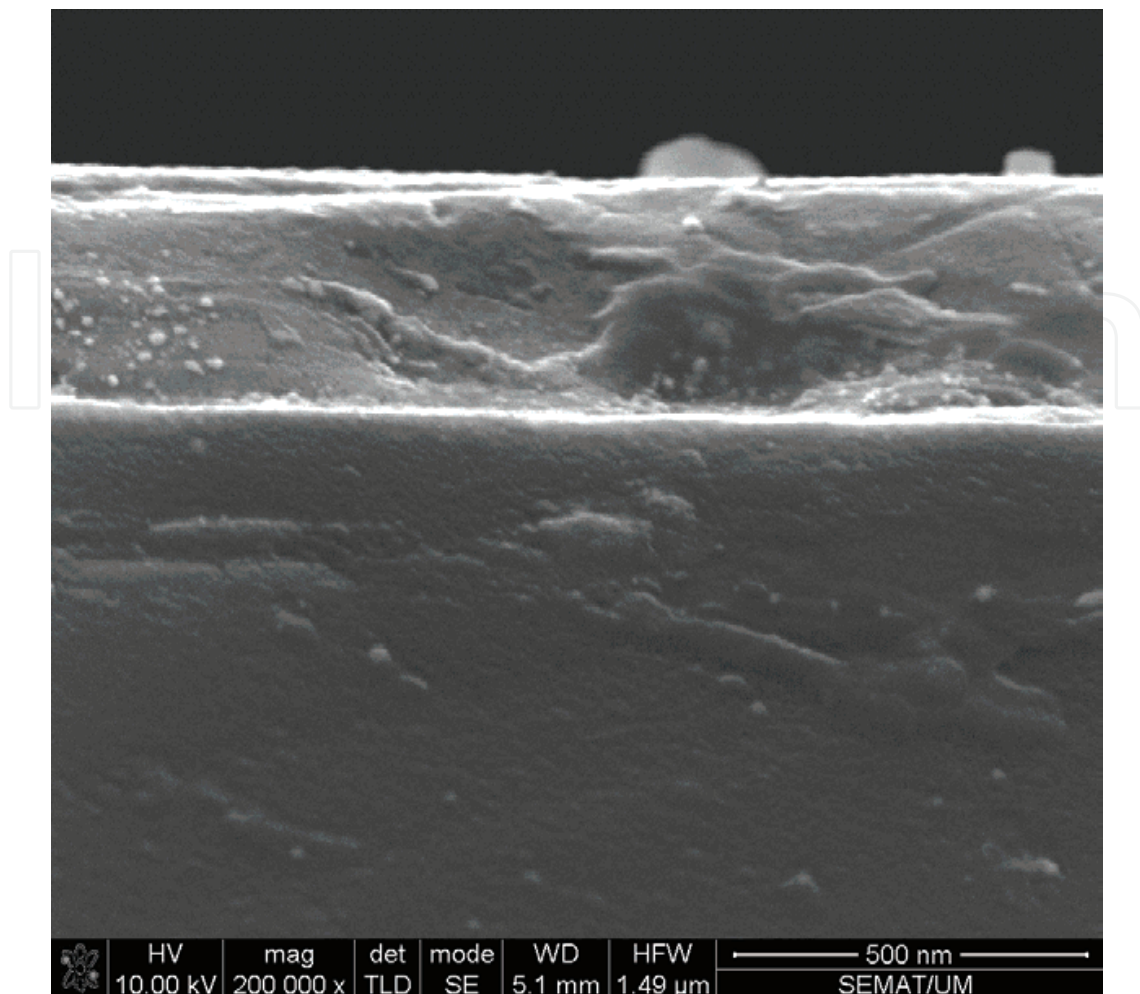


Fig. 5. Cross-section of the TiO₂:Au nanocomposite obtained by SEM.

morphological variations that may have occurred as a result of the annealing process. In order to check for clear evidences of any (micro) structural changes, which could then be used to correlate with the overall coatings behaviour, a set of XRD experiments were carried out. Diffraction profiles of all the samples, from as-deposited and annealed samples were then characterized in detail. Figure 6 shows the diffractograms obtained for the samples prepared as a function of the annealing temperature.

The set of results from the whole series of samples evidences one of the main information of this research: a clear change on the crystallographic structure of the matrix (TiO₂) and on the Au nanoparticles. The as-deposited films show an amorphous structure, without any visible traces of crystalline Au or any of the known crystalline phases of titanium oxides. However, the annealing process lead to the crystallization of the amorphous films, firstly by the detection of crystalline Au, followed by some crystallization of the TiO₂ matrix, but with this last occurring only for temperatures above 300 °C. The presence of Au, with a face centered cubic-like structure [ICDD card N° 04-0787], is evidenced for annealing temperatures above 200 °C, as evidenced by the presence of the (111) peak, localized at $2\theta \approx 38.2^\circ$, as well as the (200) peak, at $2\theta \approx 44.4^\circ$, with this last one appearing for annealing temperatures above 400 °C, exactly at the temperature where the first signs of TiO₂ crystallization have also appeared.

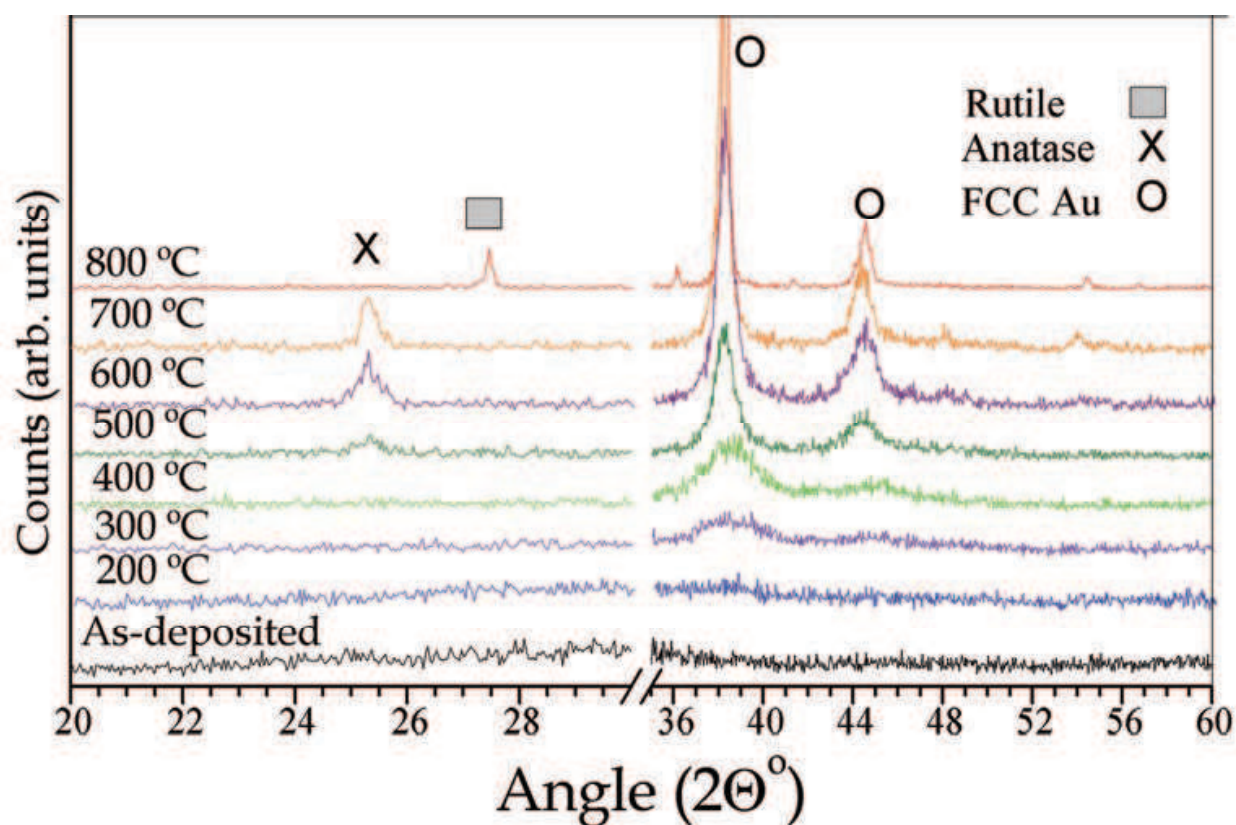


Fig. 6. X-Ray diffractogram of the nanocomposites annealing at different temperatures.

If the results of the XRD patterns are carefully looked, it can be also concluded that the initial broad Au (111) peak, which starts to be detected at an annealing temperature of 300 °C, becomes sharper. This increase of the intensity of the peaks, that also become narrower, is led by the growth of the nanoparticles, as a result of the diffusion and coalition of Au atoms. The Au clusters grow in size as the annealing temperature increases, followed by some crystallization of the amorphous oxide dielectric matrix that occurs at an annealing temperature above 400 °C. The diffraction patterns seem to indicate that the amorphous TiO₂ matrix crystallizes in the anatase form [ICDD 21-1272], as in fact suggested in similar studies where annealing of TiO₂-based films is involved (Manera et al., 2008). These results suggest that, at 500 °C, a nanocomposite film consisting of a crystalline dielectric TiO₂ matrix embedded with Au clusters was formed. At annealing temperatures above 700 °C, the TiO₂ phase changes from the anatase to the rutile [ICDD 21-1276] structure. This is in accordance with results available in the literature (Hasan et al., 2009; Martin et al., 1997). The access of this nanocomposite structure up to 500 °C should be responsible for the appearance of SPR activity, which can be used to tune some of the film properties, namely the optical ones. The role of the changes in the dielectric matrix have also been studied, and found to affect the position of the absorbance peak of the SPR. It is known that the effective dielectric function of the matrix has a direct dependence on the refractive index. A crystallization of TiO₂ structure promotes an increase in the refractive index. This change brings an increase on the dielectric function values leading a red shift of the absorbance peak. The XRD shows that the TiO₂ transforms from an amorphous phase, with a refractive index $n = 2.2$, to anatase, with a refractive index $n = 2.6$, and finally transforms to rutile that has a refractive index $n = 2.9$.

The overall set of results that were obtained in the frame of the presented work seems to indicate that the structural changes of the Au clusters may have significant importance for the SPR activity. As it is further detailed on the following sections, the first evidences of the Au crystallization (300 °C) are found to correspond to the main changes on the optical properties (reflectivity, colour and absorbance), as well.

Figure 7 shows the results of the average size (diameter) of the gold particles in the nanocomposite films, based on three different calculations, integral-Breadth, Fourier analysis and Scherrer experimental formula, applied to the XRD patterns. The values of gold particles (clusters) size range from about 2 nm at 300 °C to approximately 30 nm at 800 °C. In accordance to the results plotted in figure 7, the Au particles are confined on the nanometrical scale, which growth led by the diffusion of the Au atoms, promoted by the annealing treatments. The SPR activity and the related changes on the optical properties are directly affected by this growth. Figure 7 clearly illustrates a continuous increase of the Au particles size in this temperature range. The main SPR activity has been reported between 400 °C and 600 °C, where the average grain size is within 3 nm to 15 nm (M.Torrell et al., 2010a) At temperatures below 300 °C the size of Au clusters is too small to be considered as a crystalline structure phase dispersed on the dielectric matrix.

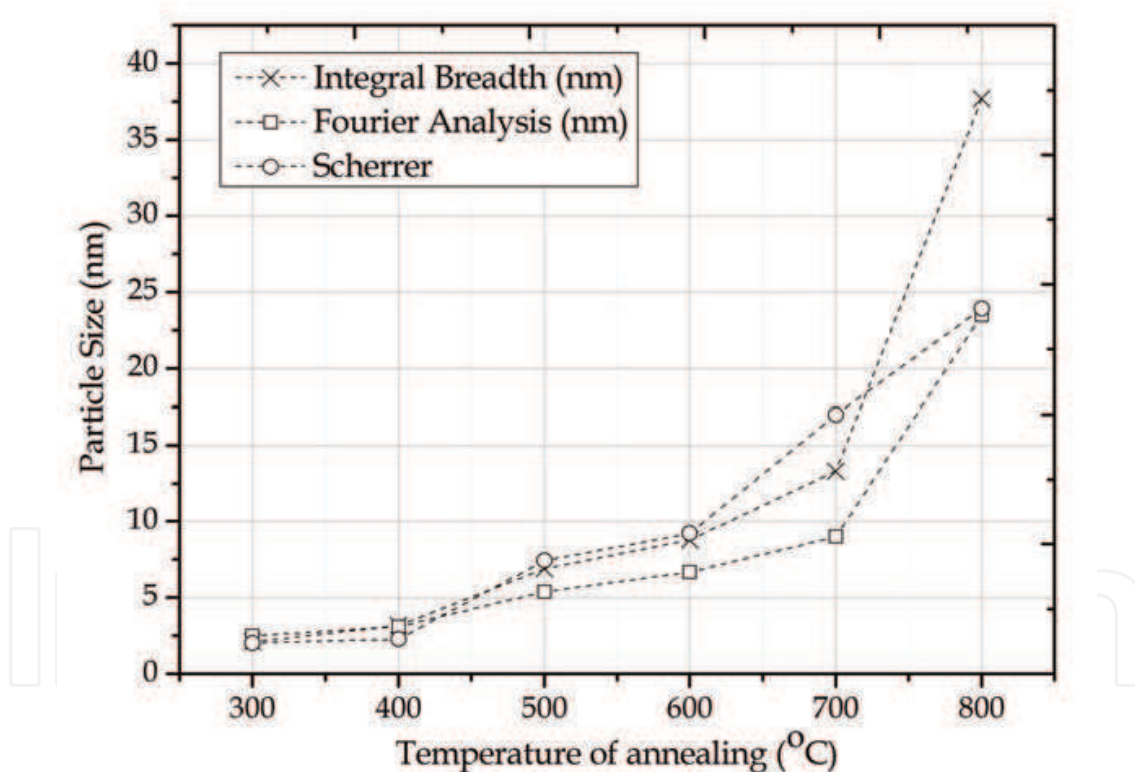
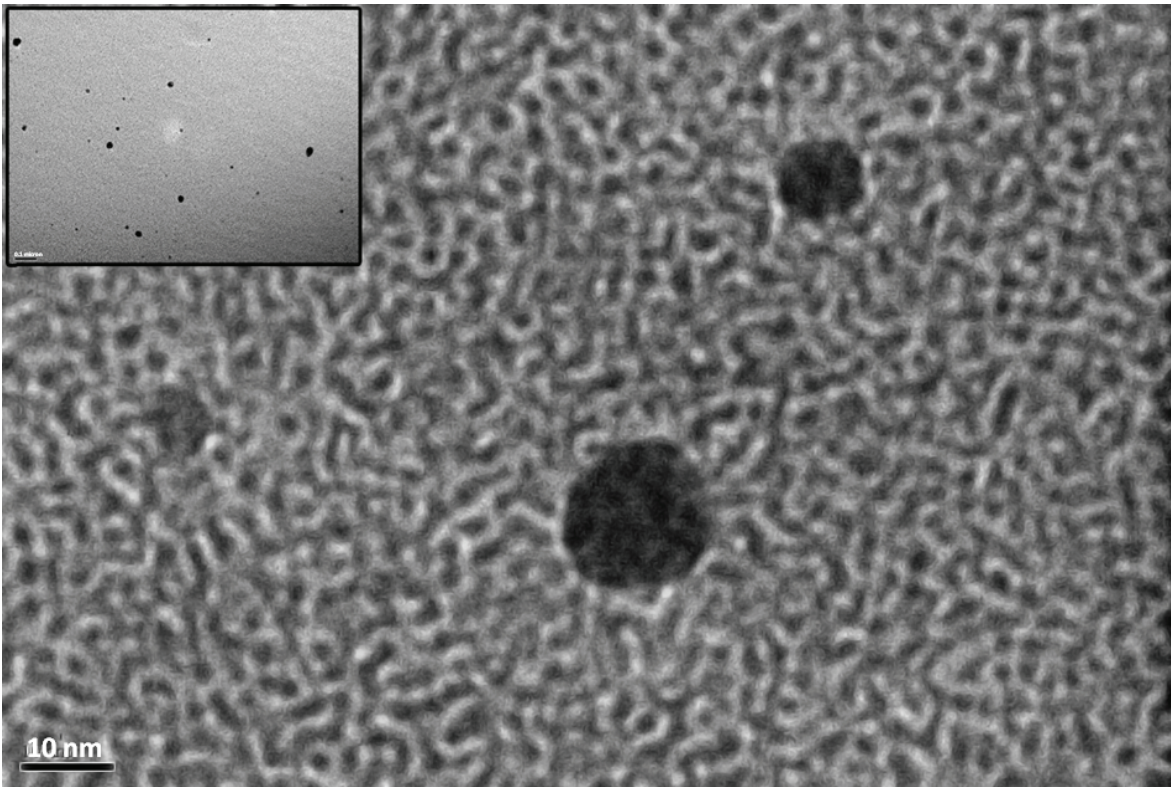
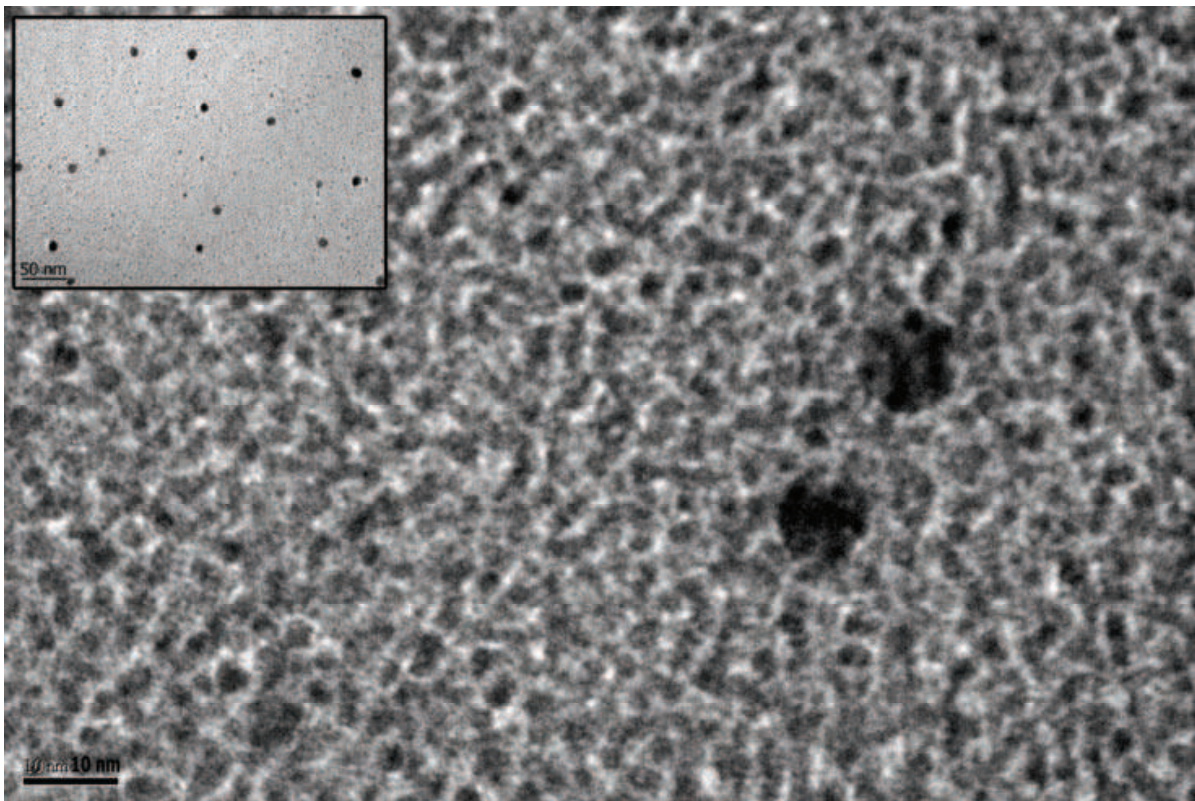


Fig. 7. Size of the Au clusters determined from the XRD Au-fcc (111) peak.

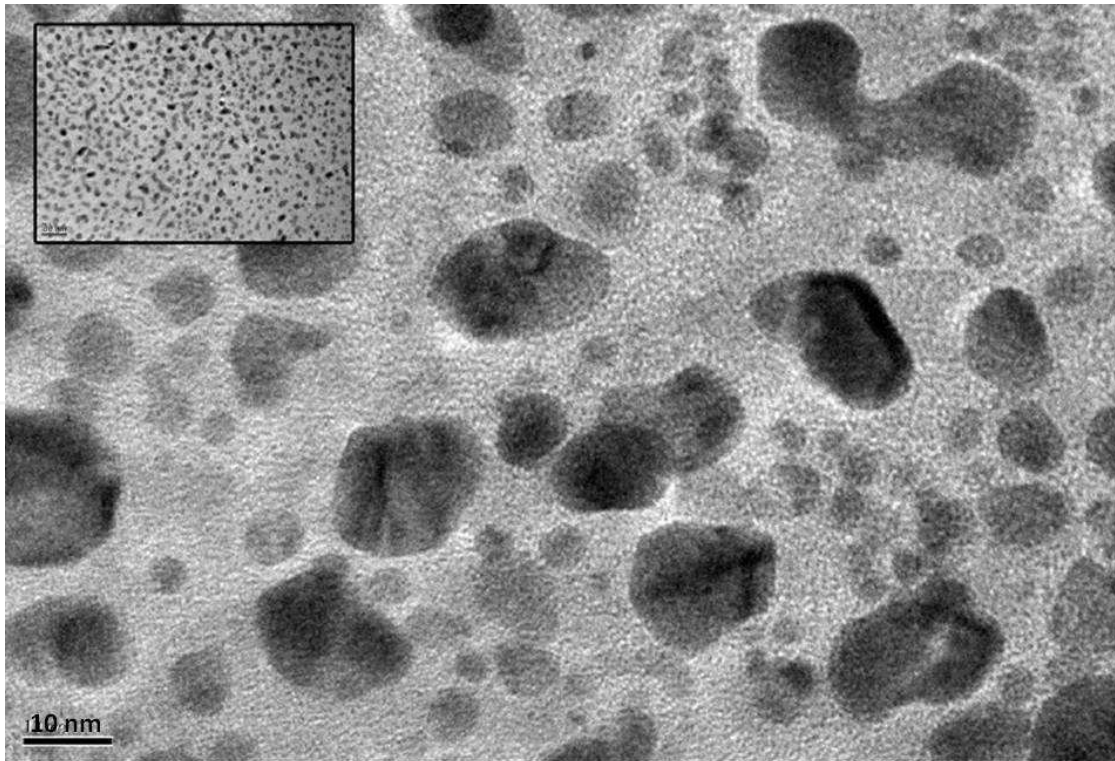
The nanoparticles growth and the matrix crystallization studied by XRD have been confirmed by transmission electron microscopy (TEM). The micrographies obtained by TEM of the samples annealed at different temperatures confirm this nanoparticles growth process that starts to be a fine atomic dispersion, and start to coalesce with the annealing treatments. Figure 8a) shows the TEM micrographies of the as-deposited sample. The Au nanoparticles are present just as an atomic dispersion of small nanoparticles in an amorphous matrix.



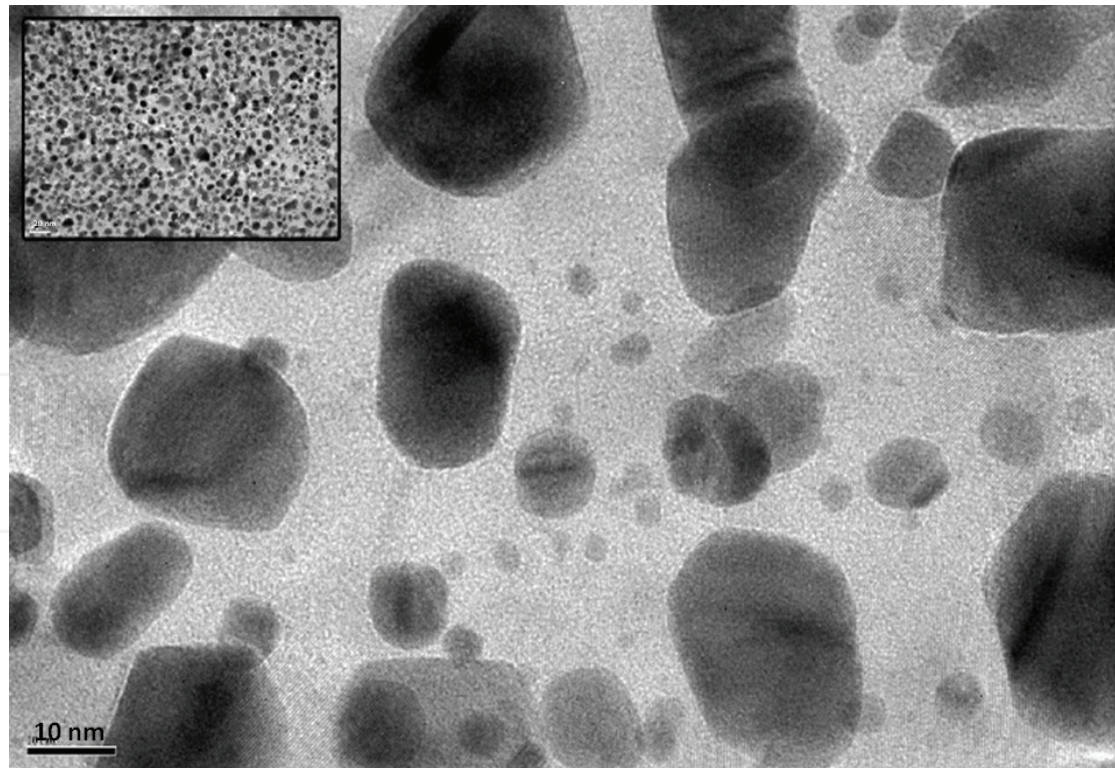
a)



b)



c)



d)

Fig. 8. TEM micrographs of the a) as-deposited sample; b) 300 °C annealed sample; c) 500 °C annealed sample and d) TEM micrographs of the 700 °C annealed sample.

Figure 8b) shows the sample annealed at 300 °C, where the Au nanoclusters start to have sizes larger than 2-3 nm, allowing their detection by XRD analysis. After annealing for 1 hour at 500 °C, the Au nanoclusters achieve average sizes around 10-12 nm. They show a homogenous dispersion on the matrix and quite symmetric spherical shape as can be observed in figure 8c). In this figure, and as it is confirmed by the electron diffraction results, the matrix starts to crystallize. The sample analysed by TEM, shown in figure 8d), was annealed at 700 °C. The nanoclusters shows sizes around 15-20 nm and a decrease on their spherical symmetry. At this annealing temperature, the XRD analysis evidences a higher degree of crystallization of the TiO₂ matrix. Analyzing the nanoclusters size by the TEM micrographs, one can start to define three different groups of samples (or different groups of annealing temperatures) that that may be correlated with their optical properties. The first group of samples (group I) may include the as-deposited sample and the one that was annealed at 300 °C, where the Au is still dispersed with very small cluster sizes in the limit of what can be considered and detected as a crystal (group I). In this first group, the TiO₂ matrix is completely amorphous. The second group (group II) includes the samples annealed from 400 to 600 °C, represented in figure 8c) by the sample annealed at 500 °C. The Au nanoclusters are homogeneously dispersed on the matrix, forming small nanocrystals with quite spherical shape. The matrix starts to crystallize as anatase. The last group (group III) includes the samples annealed at higher temperatures (700 and 800 °C). In these samples, it is detected diffusion of the clusters to the inner and outer interfaces (Figure 4). It is noticed the tendency to lose the spherical symmetry of the nanoclusters that present sizes above 20nm. The TiO₂ matrix is mostly crystallized and the anatase phase transforms to rutile.

5.2 Optical properties

The SPR effect is mainly detected by the changes on the optical properties of the nanocomposite films. The influence of the size and shape of the Au clusters embedded into the dielectric matrix can be accessed by reflectivity, absorbance and colour measurements. All these properties have been characterized and are discussed in this chapter, and correlated with the different morphologies of the films described in the previous section. Important changes of the reflectivity behaviours were found in the annealed samples, when compared to the as-deposited ones.

The interferometric optical behaviour disappears at 300 °C as can be observed in figure 9, which correlates with the change from group I samples to those from group II, as stated in the previous section. The reflectance spectra show a clear change from interference-like to intrinsic metallic like behaviour, similar to the one obtained for pure Au (Wang et al., 2006c), with the increase of the annealing temperature. The samples of groups II and III show a minimum of reflection close to 500 nm, followed by a progressive increase of the reflection intensity in the highest wavelength of the visible region of the electromagnetic spectrum.

The minimum in the reflectivity intensity has been detected at similar values of the wavelength (500 - 515 nm) with a slight blue shift with increasing annealing temperatures. Furthermore, a clear tendency for having steeper positive slope of the reflection at higher wavelengths than the minimum of the reflectance is detected. This becomes more evident with the increase of the temperature.

A clear correlation between the changes of the reflectivity and of the other optical properties with the XRD results is found. In fact, the disappearance of the interferometric features in the reflectance spectra occurs at the same annealing temperature where the Au

crystallization starts to be detected. The relatively low values of the reflectivity at shorter wavelengths are characteristic of high free electron density systems (Yate et al., 2009).

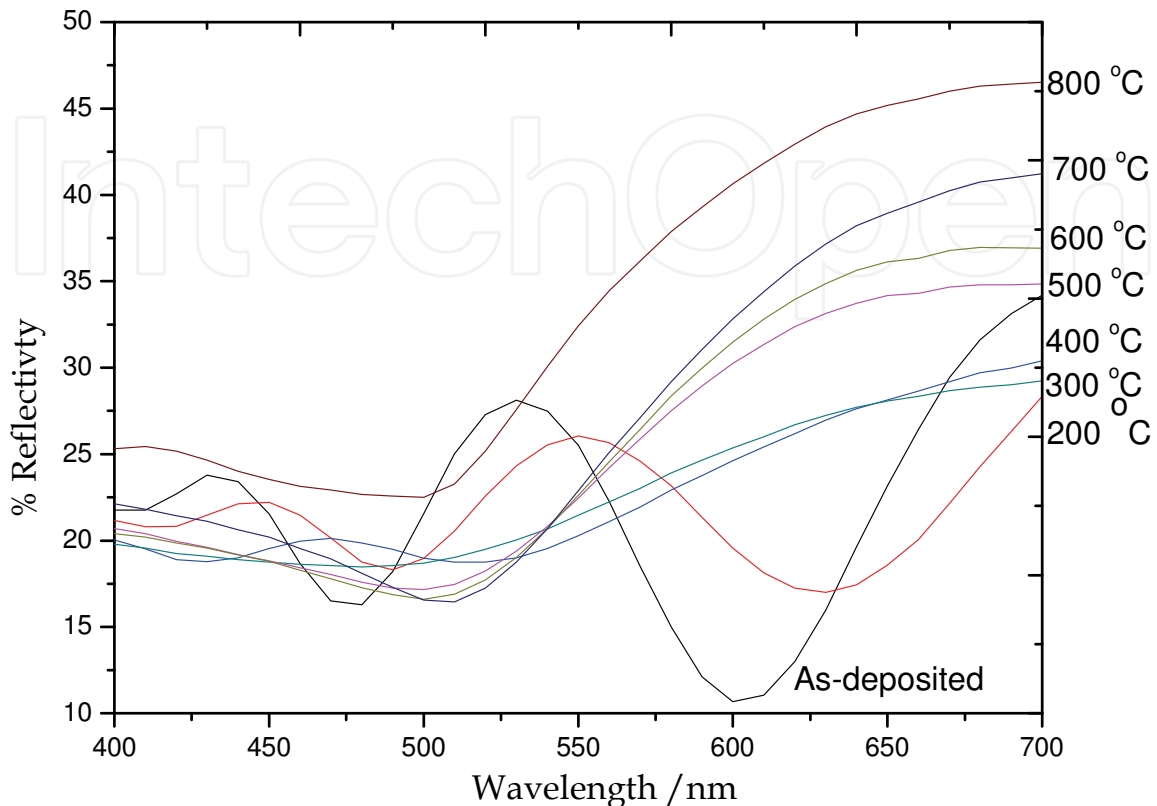


Fig. 9. Reflectivity spectra of the nanocomposites samples annealed at different temperature.

Increasing the annealing temperature, the films of group II and group III change their behaviour in comparison with the as deposited sample, from interference-like to intrinsic-like, as revealed by the surface colour tones that tend to a red-brownish colour, in comparison to the interferometric tones of the as-deposited and 200 °C annealed samples (group I), figure 10. As evidenced in figure 6, associated with the first change on the reflectivity trend, a broad peak positioned at $2\theta \approx 38.1^\circ$ was detected in the XRD pattern, which was indexed as Au (111) planes. At higher temperatures, the Au (111) XRD peaks become narrower and more intense, indicating higher crystal sizes (Figure 7), which is followed by the increase of the reflectivity and the complete vanishing of the interference bands (Figure 9).

The detailed analysis of the colour changes due to the SPR effect was studied by the CIELab colour space. The evolution of the colour parameters is shown in figure 10. The change from the interference tones towards the intrinsic red-brownish, is followed by a significant increase of the a^* parameter (redness) and a slight increase of the b^* parameter (yellowness) of the CIELab scale. The most abrupt change in the a^* parameter is detected in the 300 °C annealed sample, again coincident with the detection of Au precipitation and the transition from interference to intrinsic behaviour shown in the reflectivity curves (transition to group II samples). The magnitude of the change of the colour parameters is directly correlated with the magnitude of the change of the reflectivity values reported on figure 9.

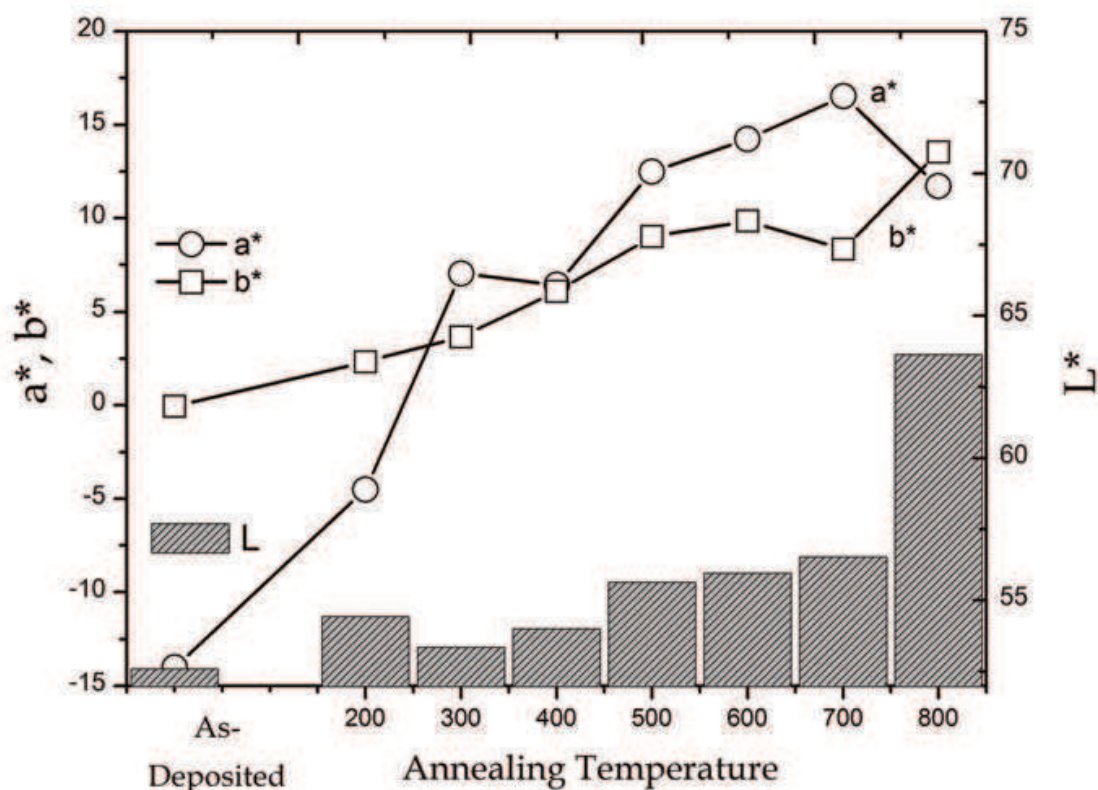


Fig. 10. Cielab colour space parameters of the as deposited and annealed samples.

In order to characterise the Surface Plasmon Resonance (SPR) activity, and correlate it with the changes in the morphology described above, the absorbance measurements ($A = \ln 1/T$) are presented in the figure 11. SPR is manifested as a distinct peak in the absorbance spectrum (Lee et al., 1999, Torrell et al., 2010c), and has been reported in several nanocomposite materials through the localization of an absorbance band on the visible wavelength range (Takele et al., 2006; Dalacu & Martinu 1999; Lee et al., 1999, Manera et al., 2008; Zakrzewska et al., 2003; J. Vosburgh & Doremus 2004.). Figure 11 shows the absorbance behaviour of the films analysed.

At the same wavelength, for the same annealed sample, higher reflectivity is linked to lower absorbance intensity. The changes in the absorbance spectra can be detected already at 300 °C, also confirming the first crystallization evidences through the precipitation of the Au clusters.

It is important to highlight that the Surface Plasmon Resonance activity or effect starts to be evident for higher annealing treatments. At temperatures of 500 °C the transmittance of the sample is close to 0 for a wide range of wavelength values, so the absorbance cannot be measured accurately. When the annealing temperature is increased, the optical density increases, but a slight red shift is also detected, together with an enhancement of the absorbance peak intensity. The absorbance peak is shifted from 587 nm to 610 nm. The peak red shift of the Au:TiO₂ samples has to be ascribed to different factors. The first is the growth of the nanoparticles, that is also related, at temperatures above 600°C to a drop on the spherical symmetry, and the variance in the dielectric constant of titanium oxide matrix that exist as different ratios of amorphous/anatase phases due to the different annealing treatments (Lee et al., 1999; Wang et al. 2005) are some of these factors. So the matrix

presents a different dielectric constant for each annealing temperature modifying the energy of the SPR absorption, located at larger wavelengths for more crystalline matrixes (higher annealing temperatures).

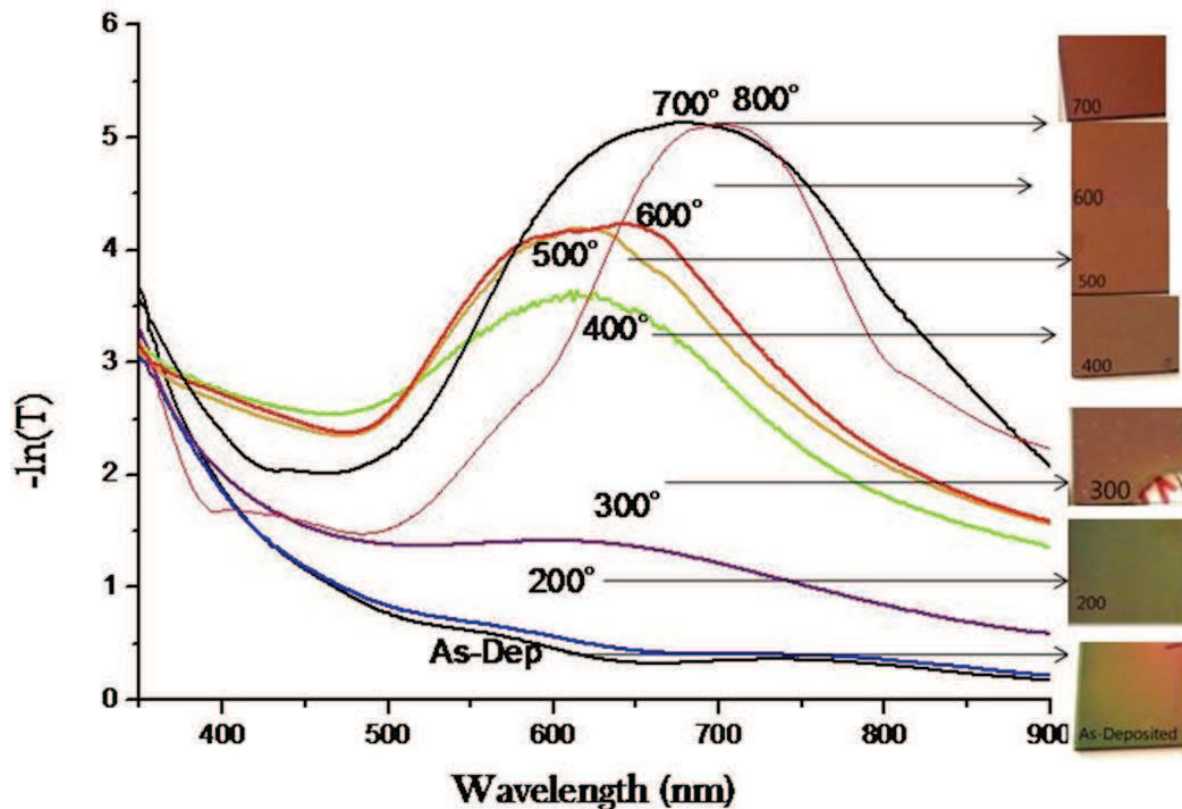


Fig. 11. Absorption spectra of the as deposited and annealed samples.

In general, the absorption peaks are relatively broad, especially those of samples annealed at low temperatures. It is well known that SPR activity depends strongly upon the morphology of the nanoparticles, namely the size and shape of the metal clusters (Lee et al., 1999; Manera et al., 2008; Dalacu & Martinu 1999). Considering a global analysis, the same three groups of samples are clearly defined in the morphological and optical results. The first group of samples (as-deposited and 200 °C annealed sample) reveal interference-like behaviour (both in reflectance and absorbance), with a surface tone characteristic of interference coloured materials (rainbow-like aspect). The samples from the second group (300, 400 500, 600 °C annealed samples) show low absorbance results and the colour tones change clearly to intrinsic-like ones, which can be characterized as light red brownish. Finally, there is a group of samples with higher SPR behaviour (samples annealed at 700 °C and higher temperatures). At these temperatures the spherical symmetry of the particles starts is lost and the cluster size is significantly larger. This higher effect of the SPR on the samples annealed at temperatures at 500° C or higher, can be clearly seen on the reflectance (Figure 9), colour coordinates (Figure 10) and absorbance (Figure 11) results. It is important to highlight that TiO₂ films do not show any of these optical changes under the same heat treatment (Dakka et al. 2000).

Once all the experimental results and the theoretical models are exposed, the reasons of the changes in the optical properties are clarified. The models indicate that the red shift of the

absorption band is produced by the change of the dielectric constant of the host material. The matrix crystallization from amorphous to the anatase and rutile phases increase the refractive index producing a change on the dielectric function that leads to the red shift, while the band broadening is caused by the break of the spherical symmetry of the nanoparticles leading to the splitting of the SPR frequency ($\omega'_{SPR} < \omega_{SPR} < \omega''_{SPR}$). The growth of elongated nanoparticles is characteristic of samples annealed at 700 - 800 °C (zone III) and it is probably related to the coalescence of smaller nanoparticles. It is important to highlight that an increase on the size of the nanoparticles leads to the growth of the SPR intensity but does not affect its position, as long as the characteristic wavelengths are much larger than $\langle R \rangle$ and the typical inter-particle distance.

In order to summarise and correlate the experimental results obtained on the morphology and optical properties of the nanocomposites, figure 12 shows the SPR absorption peak position and the Au clusters size. It's clear the correlation between the cluster grow, that it is also a parameter that is correlated with the crystallinity of the samples, and after 500°C annealed a drop on the Au particle symmetry, and the red shift of the absorption peak position.

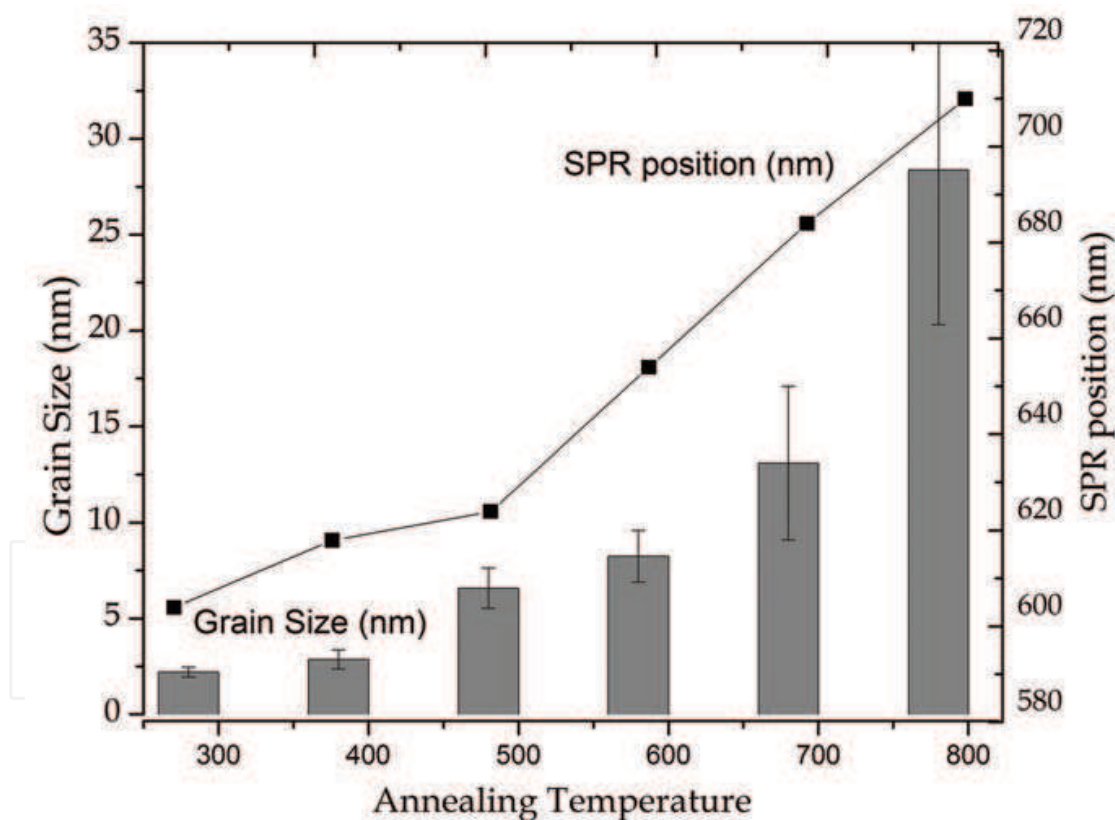


Fig. 12. SPR absorption peak red shift correlated with the Au cluster growth.

6. Conclusions

Comparing globally the overall set of results obtained for different annealing temperatures, we can conclude that the as-grown and low-temperature (zone I) annealed TiO₂/Au

composite films do not reveal a SPR absorption because there are just clusters of few Au atoms (< 1 nm, not detectable by XRD) present in these samples. Higher annealing temperatures (corresponding to zones II and III) are required to produce gold NPs and, consequently, the SPR effect on the optical spectra. Such annealing treatments affect both the TiO₂ matrix, in what concerns its crystalline/amorphous structure and phase composition, and the metallic phase, not only changing the nanoparticles size but also the shape.

The morphological modifications are evidenced by the TEM images, XRD data and the optical parameters. The experimental data are supported by the theoretical models. The red shift of the SPR band is mainly produced by the change of the dielectric constant of the host material due to its crystallization while the band broadening is caused by the break of the spherical symmetry of the nanoparticles leading to the splitting of the SPR frequency. The growth of elongated nanoparticles is characteristic of samples annealed at 700 - 800 °C (group III) and probably is related to the coalescence of smaller nanoparticles.

Presented results show that the characteristics of the SPR resonance can be tuned by choosing the appropriate annealing temperature, namely, it is possible to change the SPR position in the range of approximately 610-710 nm and also the width of the absorption band. The "one step" co-sputtering of a Ti-Au target, followed by an appropriate thermal treatment, is a useful way to produce composite TiO₂/Au films with adjustable nanostructure and, consequently, controllable SPR-related optical properties and colour.

7. Acknowledgements

The authors acknowledge the Portuguese Foundation for Science and Technology (FCT) for the financial support through project PTDC/CTM/70037/2006 funded under the program "Programa Operacional Factores de competitividade (COMPETE)" from "Quadro de Referência Estratégico Nacional (QREN)" co-participated by FEDER.

8. References

- Takele H., Greve H., Pochstein C., Zaporojtchenko V., Faupel F., (2006) Plasmonic properties of Ag nanoclusters in various polymer matrices. *Nanotechnology*, 17, 14 (Jul 2006) 3499-3505.
- Hutter E., Fendler J. H., (2004) Exploitation of Localized Surface Plasmon Resonance. *Advanced Materials*, 16(19), (Oct. 2004) 1685-1706.
- Walters G., Parkin I. P., (2008) The incorporation of noble metal nanoparticles into host matrix thin films: synthesis, characterisation and applications. *Journal of Materials Chemistry*, 19, 5 (Aug 2008) 574-590.
- Torrell M., Machado P., Cunha L., Figueiredo N.M., Oliveira J.C., Louro C., Vaz F., (2010) Development of new decorative coatings based on gold nanoparticles dispersed in an amorphous TiO₂ dielectric matrix *Surface and Coatings Technology*, 9-10, 204, (Jan 2010) 1569-1575.
- Wang C. M., Lian J., Ewing R.C. & Boatner L.A., (2006) Ion-beam implantation and cross-sectional TEM characterization of Gd₂Ti₂O₇ pyrochlore. *Nuclear Instruments and Methods*, 242 (Jan 2006) 448-451.
- Pacholski C., Kornowski A., & Weller H., (2004), *Angewandte Chemie International Edition* 43, 36, (Sept 2004) 4774-4777.

- Wu J. & Tseng C.,(2006) Photocatalytic properties of Au/ZnO nanorod composites. *Applied Catalysis B: Environment*, 66,(June 2006) 51-57.
- Li Y., Hu Y., Peng S., Lu G.,& Li S., (2009) *Journal Physical Chemistry. C* 113,21, (2009) 9352-9358.
- Atashbar M. Z., Sun H. T., Gong B., Wlodarski W., & Lamb R. (1998), XPS study of Nb-doped oxygen sensing TiO₂ thin films prepared by sol-gel method. *Thin Solid Films*. 326, (Aug. 1998) 238-244.
- Walton R. M., Dwyer D. J., Schwank J. W., & Gland J. L., (1998) Gas sensing based on surface oxidation/reduction of platinum-titania thin films I. Sensing film activation and characterization. *Applied Surface Science* 125, (Feb 1998) 187-198.
- Cho S., Lee S., Oh S., Park S. J., Kim W. M., Cheong B., Chung M., Song K. B., Lee T. S., Kim S. G. (2000) Optical properties of Au nanocluster embedded dielectric films. *Thin Solid Films*, 377-378,(Dec 2000) 97-102.
- F. Hache, D. Richard, C. Flytzanis, and K. Kreibig, The Optical Kerr Effect in Small Metal Particles and Metal Colloids - the Case of Gold. *Applied Physics A: Materials Science & Processing* 47, 4 (Jul 1988) 347-357.
- Kim K., Lee H. B., Yoon J. K., Shin D. & Shin K. S. (2010), Surface-Enhanced Raman Scattering on Aggregates of Platinum Nanoparticles with Definite Size. *Journal Physical Chemistry C* 114, (Oct 2010) 13589-13595.
- Dalacu D., Martinu L., (1999) Spectroellipsometric characterization of plasma-deposited Au/fluoropolymer nanocomposite films, *Journal of Vacuum Science Technology A* 17(3), (Feb. 1999) 877-883.
- Dalacu D., Martinu L., (2000) Spectroellipsometric characterization of plasma-deposited Au/SiO₂ nanocomposite films, *Journal of Applied. Physics* 87(1), (Aug. 2000) 228- 236.
- Bohren C. F. & Huffman D. R., Absorption and Scattering of Light by Small Particles, Wiley Professional Paperback Edition, New York, (1998).
- Deng H., Yang D., Chen B. & Lin C. W., (2008) Simulation of surface plasmon resonance of Au-WO_{3-x} and Ag-WO_{3-x} nanocomposite films. *Sensors and Actuators B: Chemical* 134, (Apr. 2008) 502-509.
- Matsuoka J., Yoshida H., Nasu H. & Kamiy K., Preparation of gold microcrystal-doped TiO₂, ZrO₂ and Al₂O₃ films through sol-gel process. *Journal of Sol-Gel Science and Technology* 9,2, (1997) 145-155.
- Liao H. B., Xiao R. F., Fu J. S. & Wong G. K. L, (1997) Large third-order nonlinear optical susceptibility of Au-Al₂O₃ composite films near the resonant frequency. *Applied Physics B: Lasers and Optics* 65, (1997) 673-676.
- Mandal S. K., Roy R. K. & Pal A. K., (2002) Surface plasmon resonance in nanocrystalline silver particles embedded in SiO₂ matrix. *Journal of Physics D: Applied Physics* 35, (Sept. 2002) 2198-2205.
- Sella C., Chenot S., Reillon V. & Berthier S., (2009) Influence of the deposition conditions on the optical absorption of Ag-SiO₂ nanocermet thin films. *Thin solid films* 517,(Aug. 2008) 5848-5854.
- P. Zhou, H. Y. You, J. H. Jia, J. Li, T. Han, S. Y. Wang, R. J. Zhang, Y. X. Zheng and L. Y. Chen, (2004) Concentration and size dependence of optical properties of Ag:Bi₂O₃

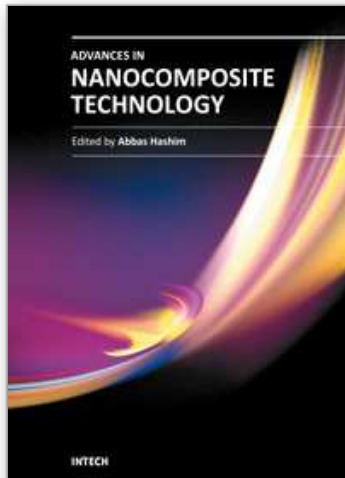
- composite films by using the co-sputtering method. *Thin solid films* 455-456, (Aug. 2005) 605-608.
- Cho S.H., Lee S., Ku D. Y., Lee T. S., Cheong B., Kim W.M., Lee K.S., (2004) Growth behavior and optical properties of metal-nanoparticle dispersed dielectric thin films formed by alternating sputtering, *Thin solid films* 447-448 (Jan. 2004) 68-73.
- Liz-Marzán L.M., (2004) Nanometals: Formation and Color, *Materials Today* 7,2 (Dec. 2004) 26-31.
- Wang C.M., Shutthanandan V., Zhang Y., Thevuthasan S., Thomas L. E., W(2009) eber W. J., Duscher G. (2006) Atomic level imaging of Au nanocluster dispersed in TiO₂ and SrTiO₃, *Nuclear Instruments and Methods Physical Research Section B*, 242 (Jan. 2006) 448-450.
- Armelaio L., Barreca D., Bottaro G., Gasparotto A., Gross S., Maragno C., Tondello E., (2006) Recent trends on nanocomposites based on Cu, Ag and Au clusters: A closer look, *Coordination Chemical Review* 250,11-12 (2006) 1294-1314.
- Navinsek B., Panjan P., Milosev I., (1999) PVD coatings as an environmentally clean alternative to electroplating and electroless processes, *Surface and Coating Technology*. 116-119 (Sept. 1999) 476-487
- Fenker M., Jackson N., Spolding M., Nicole P., Schönhute K., Gregory G., Hovsepian P.E., Munz W.D., (2004) Corrosion performance of PVD-coated and anodised materials for the decorative market, *Surface and Coatings Technology* 188-189 (2004) 466- 472.
- Mie. G. (1908) Beiträge zur Optik Trüber Medien, speziell Kolloidaler Metallösungen. *Ann. Phys.* 25 (1908) 377-452.
- H. Baida, P. Billaud, S. Marhaba, D. Christofilos, E. Cottancin, Crut A., Lermé J., Maioli P., Pellarin M., Broyer M., Del Fatti N., Vallée F., Sánchez-Iglesias A., Pastoriza-Santos I. & Liz-Marzán L. M., (2009) Quantitative Determination of the Size Dependence of Surface Plasmon Resonance Damping in Single Ag@SiO₂ Nanoparticles. *Nanoletters* 9 (2009) 3463-3469.
- Rodríguez-Fernández J., Novo C., Myroshnychenko V., Funston A. M., Sánchez-Iglesias A., Pastoriza-Santos I., Pérez-Juste J., García de Abajo F. J., Liz-Marzán L. M., & Mulvaney P., (2009) Spectroscopy, Imaging, and Modeling of Individual Gold Decahedra. *Journal of Physical Chemistry C*. 113, (Oct. 2009) 18623-18631.
- Landau L. D. & Lifshitz E. M., *Electrodynamics of Continuous Media*, Pergamon, Oxford (1984).
- Ung T., Liz-Marzan L. M., & Mulvaney P., (2001) Optical Properties of Thin Films of Au@SiO₂ Particles. *Journal of Physical Chemistry. B*, 105, (Apr. 2001) 3441-3452.
- Song G. B., Liang J. K., Liu F. S., Peng T. J., & Rao G. H.. (2005) Preparation and phase transformation of anatase-rutile crystals in metal doped TiO₂/muscovite nanocomposites. *Thin Solid Films*. 491 (2005) 110-116.
- Genzel L., Kreibitz U., *Zeitschrift Für Physik B Condensed Matter* 37, (1980) 93-101.
- Shalaev V. M., *Non.linear Optics of Random Media*, Springer, Berlin, (2000).
- Vasilevskiy M. I. & Anda E. V. (1996), Effective dielectric response of semiconductor composites, *Physical Review. B*. 54, (Aug. 1996) 5844-5851.
- Vasilevskiy M. I., (2000), Effective Dielectric response of composites containing uniaxial inclusions, *Physical Status Solidi B*, 219, (May 2000) 197-204.

- Torrell M., Cunha L., Kabir Md. R., Cavaleiro A., Vasilevskiy M.I., Vaz F. Nanoscale color control of TiO₂ films with embedded Au nanoparticles, *Material Letters*. 64, 23 15, (2010) 2624-2626.
- Barradas N.P., Jeynes C., Webb R.P., (1997) Simulated annealing analysis of Rutherford backscattering data, *Applied Physics Letter* 71, (May 1997) 291-293.
- Gurbich A.F. (1997) Evaluation of non-Rutherford proton elastic scattering cross section for oxygen. *Nuclear Instruments and Methods in Physics Research Section B*. 129 (Apr. 1997) 311-316.
- Alves E., Franco N., Barradas N. P., Nunes B., Lopes J., Cavaleiro A., Torrell M., Cunha L., & Vaz F. (2011). Structural and optical studies of Au doped titanium oxide films. *Nuclear Instruments and Methods in Physics Research Section B: Beam Interactions with Materials and Atoms*. In Press (2011). Accepted Manuscript.
- Armelao L., Barreca D., Bottaro G., Gasparotto A., Gross S., Maragno C., Tondello E., (2006) Recent trends on nanocomposites based on Cu, Ag and Au clusters: A closer look, *Coord. Chem. Rev.* 250(11-12) (2006) 1294-1314
- Manera M.G., Spadavecchia J., Buso D., de Julian Fernandez C., Mattei G., Martucci A., Mulvaney P., Pérez-Juste J., Rella R., Vasanelli L., Mazzoldi P., (2008) Thin films of TiO₂ nanocrystals with controlled shape and surface coating for surface plasmon resonance alcohol vapour sensing, *Sensors and Actuators, B* 132(1) (2008) 107-115.
- Hasan M., Haseeb A., Saidur R., Masjuki H., Hamdi M., (2009) Influence of substrate and annealing temperatures on optical properties of RF-sputtered TiO₂ thin films, *Opt. Mater.* (2009) In Press. doi:10.1016/j.optmat.2009.07.011.
- Martin N., Rousselot C., Rondot D., Palmino F., Mercier R., (1997) Microstructure modification of amorphous titanium oxide thin films during annealing treatment, *Thin solid films*. 300 (1-2) 113-121.
- Wang C.M., Shutthanandan V., Zhang Y., Thevuthasan S., Thomas L. E., Weber W. J., Duscher G., (2006) Atomic level imaging of Au nanocluster dispersed in TiO₂ and SrTiO₃, *Nuclear Instruments and Methods in Physics Research Section B*. 242 (2006) 448-450.
- Yate L., Martínez-de-Olcoz L., Esteve J., Lousa A., (2009) Control of the bias voltage in d.c. PVD processes on insulator substrates, *Vacuum*. 83(10) (2009) 1287-1290.
- Lee M., Chae L., Lee K.C., (1999) Microstructure and surface plasmon absorption of sol-gel-prepared Au nanocluster in TiO₂ thin film, *Nanostructured Materials* 11(2) (1999) 195-201.
- M. Torrell, L. Cunha, A. Cavaleiro, E. Alves, N. P. Barradas, and F. Vaz, (2010) "Functional and optical properties of Au:TiO₂ nanocomposite films: The influence of thermal annealing," *Applied Surface Science* 256,22, (2010) 6536-6542
- Zakrzewska K., Radecka M., Kruk A., Osuch W., (2003) Noble metal/titanium dioxide nanocermet for photoelectrochemical applications, *Solid State Ionic* 157(1-4) (2003) 349-56.
- Vosburgh J., Doremus R.H., Optical absorption spectra of gold nano-clusters in potassium borosilicate glass, *J. Non-Cryst. Solids* 349 (2004) 309-314.

- Wang J., Lau W.M., Li Q., (2005) Effects of particle size and spacing on the optical properties of gold nanocrystals in alumina, *Journal of Applied Physics* 97(11) (2005) 114303-114308.
- Dakka A., Lafait J., Abd-Lefdil M., Sella C., Maaza M., (2000) *Eur. Phys. Journal of Applied Physics* 9 (2000) 105-114.

IntechOpen

IntechOpen



Advances in Nanocomposite Technology

Edited by Dr. Abbass Hashim

ISBN 978-953-307-347-7

Hard cover, 374 pages

Publisher InTech

Published online 27, July, 2011

Published in print edition July, 2011

The book “Advances in Nanocomposite Technology” contains 16 chapters divided in three sections. Section one, “Electronic Applications”, deals with the preparation and characterization of nanocomposite materials for electronic applications and studies. In section two, “Material Nanocomposites”, the advanced research of polymer nanocomposite material and polymer-clay, ceramic, silicate glass-based nanocomposite and the functionality of graphene nanocomposites is presented. The “Human and Bioapplications” section is describing how nanostructures are synthesized and draw attention on wide variety of nanostructures available for biological research and treatment applications. We believe that this book offers broad examples of existing developments in nanocomposite technology research and an excellent introduction to nanoelectronics, nanomaterial applications and bionanocomposites.

How to reference

In order to correctly reference this scholarly work, feel free to copy and paste the following:

Marc Torrell Faro, Mikhail I. Vasilevskiy, Albano Cavaleiro and Filipe Vaz (2011). Nanocomposite Thin Films Resulting from Au Nanoclusters Dispersed in Titanium Oxide Dielectric Matrixes: the Surface Plasmon Resonance Effect, *Advances in Nanocomposite Technology*, Dr. Abbass Hashim (Ed.), ISBN: 978-953-307-347-7, InTech, Available from: <http://www.intechopen.com/books/advances-in-nanocomposite-technology/nanocomposite-thin-films-resulting-from-au-nanoclusters-dispersed-in-titanium-oxide-dielectric-matri>

INTECH
open science | open minds

InTech Europe

University Campus STeP Ri
Slavka Krautzeka 83/A
51000 Rijeka, Croatia
Phone: +385 (51) 770 447
Fax: +385 (51) 686 166
www.intechopen.com

InTech China

Unit 405, Office Block, Hotel Equatorial Shanghai
No.65, Yan An Road (West), Shanghai, 200040, China
中国上海市延安西路65号上海国际贵都大饭店办公楼405单元
Phone: +86-21-62489820
Fax: +86-21-62489821

© 2011 The Author(s). Licensee IntechOpen. This chapter is distributed under the terms of the [Creative Commons Attribution-NonCommercial-ShareAlike-3.0 License](#), which permits use, distribution and reproduction for non-commercial purposes, provided the original is properly cited and derivative works building on this content are distributed under the same license.

IntechOpen

IntechOpen